




## $M_{\bullet} - \sigma$ relation in spherical systems

D. BHATTACHARYYA and A. MANGALAM\* 

Indian Institute of Astrophysics, Bangalore 560 034, India.

\*Corresponding author. E-mail: mangalam@iiap.res.in

MS received 15 August 2017; accepted 25 September 2017; published online 9 February 2018

**Abstract.** To investigate the  $M_{\bullet} - \sigma$  relation, we consider realistic elliptical galaxy profiles that are taken to follow a single power-law density profile given by  $\rho(r) = \rho_0(r/r_0)^{-\gamma}$  or the Nuker intensity profile. We calculate the density using Abel's formula in the latter case by employing the derived stellar potential; in both cases. We derive the distribution function  $f(E)$  of the stars in the presence of the supermassive black hole (SMBH) at the center and hence compute the line-of-sight (LoS) velocity dispersion as a function of radius. For the typical range of values for masses of SMBH, we obtain  $M_{\bullet} \propto \sigma^p$  for different profiles. An analytical relation  $p = (2\gamma + 6)/(2 + \gamma)$  is found which is in reasonable agreement with observations (for  $\gamma = 0.75 - 1.4$ ,  $p = 3.6 - 5.3$ ). Assuming that a proportionality relation holds between the black hole mass and bulge mass,  $M_{\bullet} = f M_b$ , and applying this to several galaxies, we find the individual best fit values of  $p$  as a function of  $f$ ; also by minimizing  $\chi^2$ , we find the best fit global  $p$  and  $f$ . For Nuker profiles, we find that  $p = 3.81 \pm 0.004$  and  $f = (1.23 \pm 0.09) \times 10^{-3}$  which are consistent with the observed ranges.

**Keywords.** Galaxies: bulges—galaxies: elliptical—galaxies: kinematics and dynamics—galaxies: nuclei—galaxies: structure.

### 1. Introduction

It is now widely accepted that all massive galaxies have supermassive black holes at their centers. At distances close to the centers of these galaxies, stellar or gas motions are completely dominated by the gravity of the SMBH than that of the nearby stars. The relation of the SMBHs to their host galaxies can be seen by the strong correlation between the mass of SMBH and velocity dispersion  $\sigma$  of the stars in the galaxy. This is somewhat surprising because the stars are too far from the SMBH for the velocity dispersion to be affected by its gravitational field. Its origin is still a topic of debate.

The  $M_{\bullet} - \sigma$  relation is given by the equation

$$M_{\bullet} = k\sigma^p, \quad (1)$$

which was first reported by Ferrarese & Merritt (2000) with the index  $p = 4.8 \pm 0.5$ , whereas, Gebhardt *et al.* (2000) reported  $p = 3.75 \pm 0.3$ . The former used symmetric linear regression method for their analysis and in this process both the variables  $M_{\bullet}$  and  $\sigma$  had an unique error in measurements as well as intrinsic scatter, while the later used non-symmetrical least square regression, where it was assumed that  $\sigma$  had no uncertainty in

measurement and  $M_{\bullet}$  had the same the uncertainty for all. This relation is observed in ellipticals and evolved bulges. Debattista *et al.* (2013) claimed that their latest measurements indicate that there is no evidence of offset for this relation between ellipticals and classical bulges. Table 1 shows the values of the indices determined by different authors using different techniques.

There are many theoretical models proposed for explaining the  $M_{\bullet} - \sigma$  relation. Silk and Rees (1998) discussed an energy-driven flow where the energy released in accretion is used completely in the process of unbinding the mass of the galactic bulge. They modeled a protogalaxy and assumed it to be an isothermal sphere to find  $p = 5$ . King (2003) described another model based on gas accretion but with momentum-driven flow, giving  $p = 4$ . In this process, it has been assumed that cooling occurs by inverse Compton, and thereby a fraction of energy is lost to radiation while some part of the accretion energy is available for unbinding the bulge. At a point, the gas accretion stops and the black hole mass saturates; this is the maximum mass attained by gas accretion in the presence of cooling. Zhao *et al.* (2002), based on the loss cone dynamics in an isothermal halo, obtained  $p = 5$  for a model based on growth

**Table 1.** A survey of the  $M_{\bullet} - \sigma$  relation giving the historical determinations of the slopes.

$p$	Comments	References
$4.8 \pm 0.5$	12 elliptical galaxies with known $\sigma$	Ferrarese & Merritt (2000)
$3.75 \pm 0.3$	26 galaxies with measured $M_{\bullet}$ and $\sigma$	Gebhardt <i>et al.</i> (2000)
$4.72 \pm 0.36$	27 galaxies with measured $M_{\bullet}$ and $\sigma$	Merritt & Ferrarese (2001)
$4.58 \pm 0.52$	16 spirals and 20 elliptical galaxies	Ferrarese (2002)
$4.02 \pm 0.32$	31 galaxies with measured $M_{\bullet}$ and $\sigma$	Tremaine <i>et al.</i> (2002)
$4.86 \pm 0.43$	SMBHs which have resolved $r_h$	Ferrarese & Ford (2005)
$4.24 \pm 0.41$	Combination of spiral and elliptical galaxies	Gültekin <i>et al.</i> (2009)
$3.96 \pm 0.42$	25 Elliptical galaxies	Gültekin <i>et al.</i> (2009)
$4.38 \pm 0.29$	Classical bulges and ellipticals	Kormendy & Ho (2013)
$5.64 \pm 0.32$	19 late type and 53 early-type galaxies	McConnell & Ma (2013)
$5.53 \pm 0.34$	51 non-barred galaxies	Graham & Scott (2013)
$4.39 \pm 0.42$	Sample of Gültekin <i>et al.</i> (2009) with newly measured $M_{\bullet}$ and $\sigma$	Debattista <i>et al.</i> (2013)
$4.76 \pm 0.60$	32 quiescent galaxies	Batiste <i>et al.</i> (2017)
$3.90 \pm 0.93$	16 AGN host galaxies	Batiste <i>et al.</i> (2017)

by stellar ingestion. The origin of this relation is still a mystery but various models give a range  $p = 4-5$ , which is in rough agreement with observations.

From observations, it is seen that bulge mass,  $M_{\bullet} \simeq f M_b$ , where  $f = 1.259 \times 10^{-3}$  (Merritt & Ferrarese 2001). Later Marconi & Hunt (2003) and Häring & Rix (2004) found  $f = 2 \times 10^{-3}$  and  $f = (1.4 \pm 0.4) \times 10^{-3}$  respectively. For higher masses, the relation is said to be nonlinear and given by  $M_{\bullet} \propto M_b^{1.12}$  (Häring & Rix 2004) where the Jeans equation has been applied with zero anisotropy in the system to determine the velocity dispersion of 30 elliptical galaxies whose bulge masses are sourced from Magorrian *et al.* (1998). Kormendy and Ho (2013) have also found the following relation:

$$\left( \frac{M_{\bullet}}{10^9 M_{\odot}} \right) = 0.49^{+0.06}_{-0.05} \left( \frac{M_b}{10^{11} M_{\odot}} \right)^{1.17 \pm 0.08}. \quad (2)$$

Byun *et al.* (1996) introduced and calculated Nuker profiles for 57 early type galaxies from HST data. This profile is described by two power laws and matches with the observational profiles very well. Instead of conventional structural parameters such as core radius and central surface brightness, new parameters like the break radius  $r_b$ , and surface brightness,  $\mu_b$ , at that radius were used. Another parameter  $\alpha$  describes the sharpness of the break and they have calculated these parameters by applying  $\chi^2$  minimization technique to the mean surface brightness profiles of the early type galaxies. Faber *et al.* (1997) have analyzed 61 elliptical galaxies and spiral bulges from HST data and derived parameters like  $r_b$ , the intensity at that radius,  $I_b$ ,  $\sigma$  and  $L$ . Wang & Merritt (2004) and Stone & Metzger (2016) used these

results in their spherical galaxy model for deriving the distribution function while we use it to derive the empirical  $M - \sigma$  relation.

In this paper, we describe a theoretical model for calculating line-of-sight velocity dispersion for spherical systems, thereby deriving the  $M_{\bullet} - \sigma$  relation. In section 2, we discuss the nexus between the  $M_{\bullet} - \sigma$  relation and the power-law mass density index analytically, motivating the theoretical models of power-law galaxies. In section 3, we have extended the model to the case of Nuker intensity profile, which is much more generalized than the special case of a single power-law profile. Using parameters derived from the observational profiles for 12 galaxies, we have determined the  $M_{\bullet} - \sigma$  relation and the  $M_b - M_{\bullet}$  relation for the proportionality case from  $\chi^2$  analysis. We discuss our results in section 5 and present our conclusions in section 6.

## 2. Connection of $M_{\bullet} - \sigma$ relation with power law mass density of galaxies

If  $M_{\bullet}$  is proportional to  $M_b$ , then equation (1) can be written as

$$f M_b = k \sigma^p. \quad (3)$$

The total mass scales as  $\rho r^3$ , where  $\rho$  is the mass density of the galaxy and  $r$  is the distance from the center of the galaxy; similarly  $\sigma$  scales as  $\sqrt{\rho r^2}$ . Therefore, from equation (3), it can be seen that

$$\begin{aligned} \rho r^3 &\propto \rho^{\frac{p}{2}} r^p \\ \Rightarrow \rho &\propto r^{\frac{2p-6}{2-p}}. \end{aligned} \quad (4)$$

From the above relation it can be confirmed that the density follows a single power law so that

$$\gamma = \frac{2p-6}{2-p}; \text{ or equivalently } p = \frac{2\gamma+6}{2+\gamma}, \quad (5)$$

where  $\gamma$  is the power-law index. Taking typical observational values for  $p$ , we find that  $\gamma = 0.75-1.4$  gives  $p = 3.6-5.3$ . For a single power-law profile given by

$$\rho(r) = \rho_0 \left( \frac{r}{r_0} \right)^{-\gamma}, \quad (6)$$

we use Poisson's equation to calculate the stellar potential of the system

$$\nabla^2 \Phi = 4\pi G \rho, \quad (7)$$

to find a stellar potential of the form

$$\psi_{\star}(r) = \frac{4\pi G \rho_0 r_0^{\gamma} r_h^{2-\gamma}}{(2-\gamma)(3-\gamma)} \left[ 1 - \left( \frac{r}{r_h} \right)^{2-\gamma} \right]. \quad (8)$$

The total mass of stars contained within  $r_h$  is given by

$$\begin{aligned} M_{\star}(r < r_h) &= \int_0^{r_h} \rho(r) 4\pi r^2 dr \\ &= 4\pi \rho_0 r_0^{\gamma} \int_0^{r_h} r^{2-\gamma} dr \\ &= 4\pi \rho_0 r_0^{\gamma} \frac{r_h^{3-\gamma}}{3-\gamma} = 2M_{\bullet}, \end{aligned} \quad (9)$$

where  $\rho_0 r_0^{\gamma} = \frac{(3-\gamma)}{2\pi} M_{\bullet} r_h^{\gamma-3}$ , so that the stellar potential takes the form

$$\psi_{\star}(r) = \frac{2}{2-\gamma} \frac{GM_{\bullet}}{r_h} \left[ 1 - \left( \frac{r}{r_h} \right)^{2-\gamma} \right], \quad (10)$$

and the total potential is given by

$$\psi(r) = \psi_{\star}(r) + \frac{GM_{\bullet}}{r} + \psi_c, \quad (11)$$

where  $\psi_c$  is a constant which ensures that  $\psi(r)$  asymptotes to zero. We normalize the total potential in units of  $GM_{\bullet}/r_h$  so that

$$\begin{aligned} \psi &= \frac{1}{r_{\star}} + \frac{2}{2-\gamma} (1 - (r_{\star})^{2-\gamma}) + \psi_0 \\ &= x + \frac{2}{2-\gamma} (1 - (x)^{\gamma-2}) + \psi_0, \end{aligned} \quad (12)$$

where

$$r_{\star} = \frac{r}{r_h}, x = \frac{1}{r_{\star}}, \psi_0 = \frac{\psi_c}{\frac{GM_{\bullet}}{r_h}}. \quad (13)$$

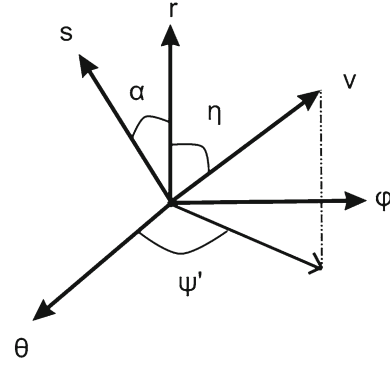


**Figure 1.** The velocity vector  $\mathbf{v}$ , LoS direction  $\hat{s}$  and the definition of the angles  $\alpha$ ,  $\eta$  and  $\psi'$  are sketched.

Next, we calculate the distribution function from Eddington's formula as

$$f(\epsilon) = \frac{1}{\sqrt{8\pi^2 m_{\star}}} \frac{d}{d\epsilon} \int_0^{\epsilon} \frac{d\rho}{d\psi} \frac{d\psi}{\sqrt{\psi - \epsilon}}, \quad (14)$$

where  $m_{\star}$  is the stellar mass which results in

$$f(\epsilon) = \frac{\gamma(3-\gamma)}{4\sqrt{2}\pi^3} \frac{1}{m_{\star}} \frac{1}{G^3 M_{\bullet}^2} g(\epsilon),$$

where

$$g(\epsilon) = \frac{d}{d\epsilon} \int_{x_1}^{x_2} \frac{x^{\gamma-1}}{\sqrt{\epsilon - x - \frac{2}{2-\gamma}(1-x^{\gamma-2})}} dx, \quad (15)$$

and  $x_1$  and  $x_2$  are the roots of the equations  $\psi(x) = 0$  and  $\psi(x) = \epsilon$  respectively.

The LoS velocity dispersion is given by (Binney & Tremaine 2008):

$$\sigma_{\parallel}^2 = \frac{\int dx_{\parallel} d^3 \mathbf{v} v_{\parallel}^2 f(x, v)}{\int dx_{\parallel} d^3 \mathbf{v} f(x, v)}. \quad (16)$$

We use  $\sigma$  in place of  $\sigma_{\parallel}$  for the rest of the paper. Consider the system to be spherical, and use polar coordinates in velocity space as (see Fig. 1),

$$v_r = v \cos \eta, v_{\theta} = v \sin \eta \cos \psi', v_{\phi} = v \sin \eta \sin \psi'. \quad (17)$$

We take the LoS (line-of-sight) direction to be an arbitrary direction,  $\hat{s}$ , which lies in the  $r - \theta$  plane making an angle  $\alpha$  with  $\hat{r}$  axis so that

$$\hat{s} = \cos \alpha \hat{r} + \sin \alpha \hat{\theta}. \quad (18)$$

The projected velocity in this plane of LoS is given by

$$\mathbf{v} \cdot \hat{s} = v_{\parallel} = v \cos \eta \cos \alpha + v \sin \eta \cos \psi' \sin \alpha. \quad (19)$$

The distance along the LoS is now  $x_{\parallel} = r \cos \alpha$ , where the perpendicular distance is  $x_{\perp} = \omega = r \sin \alpha$  and

$$x_{\parallel} = \sqrt{r^2 - r^2 \sin^2 \alpha} = \sqrt{r^2 - \omega^2}, \quad (20)$$

where  $r^2$  varies from  $\omega^2$  to  $\infty$ . We find the denominator  $D$  and the numerator  $N$  of the LoS velocity dispersion (equation (16)) separately as

$$\begin{aligned} D_1 &= \int dx_{\parallel} d^3 \mathbf{v} f(x, v) \\ &= \frac{1}{2} \int_{r^2=\omega^2}^{\infty} \frac{d(r^2)}{\sqrt{r^2 - \omega^2}} \int_{v=0}^{\sqrt{2\psi}} \int_{\eta=0}^{\pi} \int_{\psi'=0}^{2\pi} v^2 \cdot \\ &\quad dv \sin \eta d\eta d\psi' f(\varepsilon), \end{aligned} \quad (21)$$

which after substituting  $u = \omega^2/r^2$  and  $v^2 = 2(\psi - \varepsilon)$  reduces to

$$D_1 = \pi \omega J_0 \int_0^1 \frac{du}{u^2 \sqrt{\frac{1}{u} - 1}} \int_0^{\psi} d\varepsilon (2(\psi - \varepsilon))^{\frac{1}{2}} f(\varepsilon), \quad (22)$$

where  $J_0 = \int_0^{\pi} \sin \eta d\eta = 2$ . Now,

$$\begin{aligned} N_1 &= \int dx_{\parallel} d^3 \mathbf{v} v^2 f(x, v) \\ &= \frac{1}{2} \int_{r^2=\omega^2}^{\infty} \frac{d(r^2)}{\sqrt{r^2 - \omega^2}} \int_{v=0}^{\sqrt{2\psi}} \int_{\eta=0}^{\pi} \int_{\psi'=0}^{2\pi} \\ &\quad v^2 dv \sin \eta d\eta d\psi' \\ &\quad v^2 \left( \cos \eta \frac{\sqrt{r^2 - \omega^2}}{\sqrt{r^2}} + \sin \eta \cos \psi' \sqrt{\frac{\omega^2}{r^2}} \right)^2 f(\varepsilon). \end{aligned}$$

Similarly, with the same substitutions,  $N_1$  reduces to

$$\begin{aligned} N_1 &= \omega 2^{\frac{1}{2}} \left[ 2\pi J_1 \int_0^1 \frac{du \sqrt{\frac{1}{u} - 1}}{u} \int_0^{\psi} d\varepsilon (\psi - \varepsilon)^{\frac{3}{2}} f(\varepsilon) \right. \\ &\quad \left. + J_2 J_3 \int_0^1 \frac{du}{u \sqrt{\frac{1}{u} - 1}} \int_0^{\psi} d\varepsilon (\psi - \varepsilon)^{\frac{3}{2}} f(\varepsilon) \right], \end{aligned} \quad (23)$$

where

$$\begin{aligned} J_1 &= \int_0^{\pi} \sin \eta \cos^2 \eta d\eta = \frac{2}{3}, \quad J_2 = \int_0^{\pi} \sin^3 \eta d\eta = \frac{4}{3}, \\ J_3 &= \int_0^{2\pi} \cos^2 \psi' d\psi' = \pi. \end{aligned}$$

The dimensionless LoS velocity dispersion given by  $\sigma = \sqrt{\frac{N_1}{D_1}}$  for power-law galaxies is shown in Fig. 2, where we can see that the velocity dispersion is flattening out as we move outwards from the center of the galaxy. Near the center of the galaxy where the SMBH potential dominates,  $\sigma \propto 1/\sqrt{r}$ . Later it flattens out because of the dominance of the stellar potential. By finding  $\sigma$  at any radius one can verify the  $M_{\bullet} - \sigma$  relation if  $M_{\bullet}$  is known.

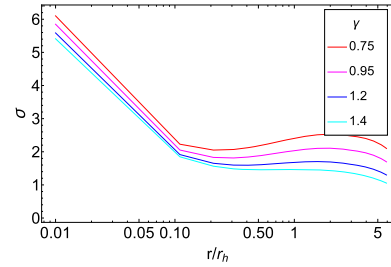


**Figure 2.** The dimensionless  $\sigma$  is plotted against projected  $r/r_h$  for various power-law indices  $\gamma$ .

From the definition, equation (9),  $r_h$  for a single power-law galaxy can be written as

$$r_h = \left( \rho_0 r_0^\gamma \frac{2\pi}{3 - \gamma} \frac{1}{M_{\bullet}} \right)^{\frac{1}{\gamma-3}}. \quad (24)$$

The total mass out to the bulge can be calculated to be

$$\int_0^{r_s} \rho_0 \left( \frac{r_0}{r} \right)^\gamma 4\pi r^2 dr = M_s, \quad (25)$$

where,  $r_s$  is the radius of the central bulge. Therefore,  $\rho_0 r_0^\gamma$  can be written as

$$\rho_0 r_0^\gamma = \frac{M_s}{\int_0^{r_s} 4\pi r^{2-\gamma} dr} = \frac{M_s(3 - \gamma)}{4\pi r_s^{3-\gamma}}. \quad (26)$$

For a range of black hole mass ( $M_{\bullet} = 10^6$  to  $10^9 M_{\odot}$ ) our calculated  $\sigma(M_s, \gamma)$ ,  $\log k(M_s, \gamma)$  and  $p(\gamma)$  (which is observationally within 4–5) are shown in Fig. 3, where,  $M_s$  varies from  $10^{10}$  to  $10^{14} M_{\odot}$ ,  $r_s$  varies from 1–10 kpc and  $\gamma$  varies from 0.75 to 1.5. We can see that for a fixed value of  $\gamma$ ,  $p$  is independent of the value of  $M_s$ . We find the range of  $p$  to be 3.6–5.3, which agrees well with the observations. Figure 3(b) shows a plot of  $\log k(M_s, \gamma)$ ; a change in  $M_s$  for a fixed value of  $\gamma$  affects the intercept though the slope is unchanged. To explain the nature of these plots, we write equation (1) as

$$M_{\bullet} = \left( \frac{M_s}{2} \right)^{\frac{1}{\gamma-2}} r_s^{\frac{\gamma-3}{\gamma-2}} (\sigma_h^2 G)^{-\frac{\gamma-3}{\gamma-2}} \sigma^{\frac{2(\gamma-3)}{\gamma-2}}, \quad (27)$$

where,  $\sigma_h$  is the value of dimensionless  $\sigma$  at  $3r_h$ . From equation (27) we see that the constant  $k$  depends on  $\gamma$ ,  $r_s$  and  $M_s$ , but the index  $p$  of the  $M_{\bullet} - \sigma$  relation depends only on  $\gamma$  which clearly explains the nature of the plots in Figures 3(a) and 3(b).

The contour plot of  $\sigma_{200}$  (see Fig. 3) at  $3r_h$  for different power laws by varying  $M_s$  and  $M_{\bullet}$  for a fixed  $r_s = 10^4$  pc is shown in Fig. 3. By selecting a physical and observed range for  $\sigma$ , one can obtain the allowed  $M_{\bullet} - M_s$  combinations for those systems.

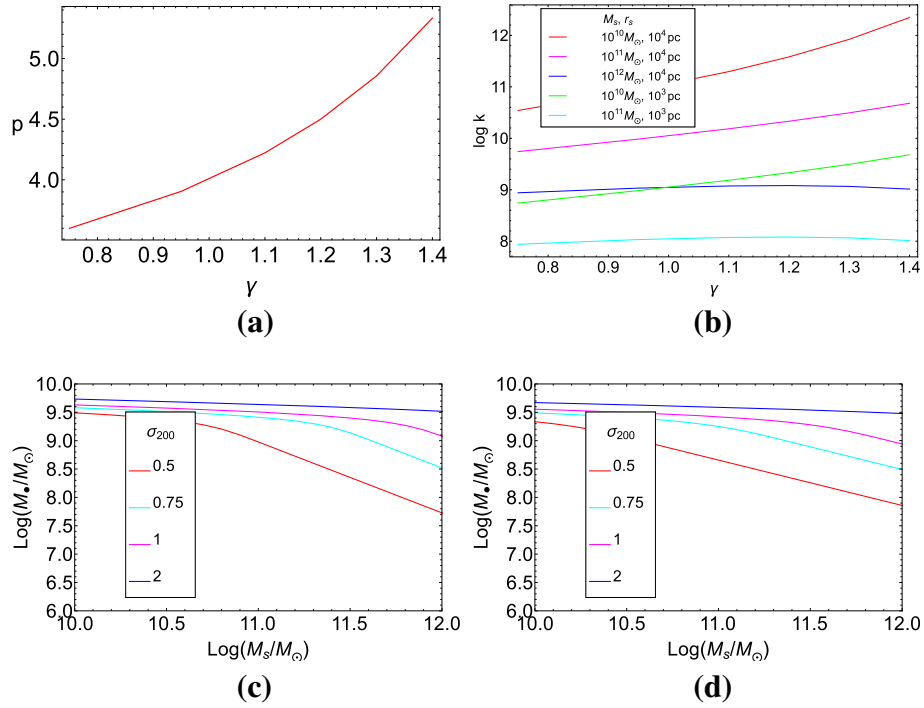


**Figure 3.** Plot of  $p(\gamma)$  (a) and plot of  $\log k(M_s)$  (b) for different values of  $\gamma$  for different  $M_s - r_s$  combinations. Contour plot of  $\sigma_{200}$  at  $3r_h$  for different power laws ( $\gamma = 1.2$  (c) and  $\gamma = 0.75$  (d)) by varying  $M_s$  for different values of  $M_\bullet$  for a fixed  $r_s = 10^4 \text{ pc}$ .

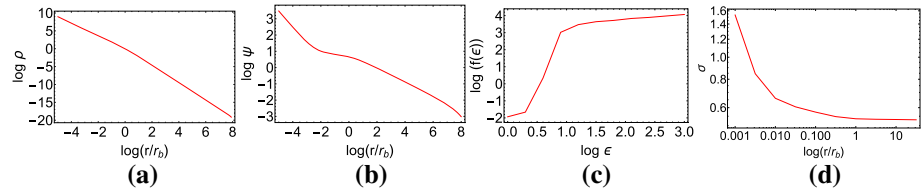


**Figure 4.** The density, total potential, distribution function and velocity dispersion plots, (a)–(d) for  $f = 0.0012$  for NGC 3115.

### 3. Spherical galaxies following Nuker profile of intensity

The Nuker profile used to fit the observational luminosity data is given by

$$I(\xi) = I_b 2^{\frac{(\beta-\Gamma)}{\alpha}} \xi^{-\Gamma} (1 + \xi^\alpha)^{-\frac{(\beta-\Gamma)}{\alpha}}, \quad (28)$$

where  $\xi = \frac{R}{r_b}$ ,  $r_b$  is the break radius,  $I_b$  is the intensity at the break radius,  $\Gamma$  is the inner slope and the outer slope is  $\beta$ . The visual mass-to-light ratio is denoted by  $\Upsilon_v$  (assuming  $H_0 = 80 \text{ km s}^{-1} \text{ Mpc}^{-1}$ ) and  $\mu_b$  is the surface brightness in visual magnitudes  $\text{arcsec}^{-2}$  at  $r_b$ . The quantity  $\mu$  represents the apparent magnitude of the equivalent total light observed in a square arcsec at different points in the distribution and it can be related to the physical surface brightness profile through (Binney & Merrifield 1998)

$$\mu = -2.5 \log I + C, \quad (29)$$

where  $C$  is a constant. If the intensity is measured in units of  $L_\odot \text{ pc}^{-2}$ , then the constant can be calculated from the distance modulus formula and it is given as

$$C = -5 \log_{10}(\delta\theta) + M_\odot^{\text{abs}} - 5, \quad (30)$$

where  $\delta\theta$  is  $1'' = \frac{1}{206265}$  radians and the solar absolute magnitude,  $M_\odot^{\text{abs}}$  is 4.83 so that  $I_b(\mu_b)$  can be calculated. The stellar mass density profile was computed via Abel's inversion equation as

$$\rho(r) = \Upsilon_v j(r) = -\frac{\Upsilon_v}{\pi} \int_r^\infty \frac{dI}{dR} \frac{dR}{\sqrt{R^2 - r^2}}, \quad (31)$$

where  $j(r)$  is the luminosity density. The stellar potential  $\psi_*$  is calculated from the stellar mass density as follows (see Fig. 4(a)):

$$\psi_*(r) = \frac{4\pi G}{r} \int_0^r \rho(r')r'^2 dr' + 4\pi G \int_r^\infty \rho(r')r' dr'. \quad (32)$$

As before the gravitational potential  $\psi(r) = -\Phi(r)$  is the total potential given by (see Fig. 4(b))

$$\psi(r) = \psi_*(r) + \frac{GM_{\text{BH}}}{r}. \quad (33)$$

The density follows the same profile (double power law) as intensity (see Fig. 4(a)), where we see the total potential (see Fig. 5(b)) being dominated by SMBH potential at the inner radii and is dominated by the stellar potential as we move outwards from the center. Again we use the Eddington's formula, equation (14), to calculate  $f(\epsilon)$  as shown in Fig. 4(c). The denominator of the LoS velocity dispersion can be written as

$$\begin{aligned} D_2(\alpha, \beta, \Gamma, \Upsilon, r_b, \mu_b, L, f) &= \int dx_{\parallel} d^3 \mathbf{v} f(x, v) \\ &= \int_{r=\omega}^{\infty} \frac{r dr}{\sqrt{r^2 - \omega^2}} \int_{v=0}^{\sqrt{2\psi}} \int_{\eta=0}^{\pi} \int_{\psi'=0}^{2\pi} \\ &\quad \times v^2 dv \sin \eta d\eta d\psi' f(\epsilon). \end{aligned} \quad (34)$$

By replacing the variable  $r$  by  $1/u$ , the denominator can finally be written as

$$\begin{aligned} D_2(\alpha, \beta, \Gamma, \Upsilon, r_b, \mu_b, L, f) &= 2^{\frac{3}{2}} 2\pi J_0 \\ &\int_{u=0}^{1/\omega} \frac{du}{u^2 \sqrt{1 - \omega^2 u^2}} \int_{\epsilon=0}^{\psi} (\psi(u) - \epsilon)^{\frac{1}{2}} f(\epsilon) d\epsilon. \end{aligned} \quad (35)$$

The numerator  $N_2$  of the LoS velocity dispersion is

$$\begin{aligned} N_2(\alpha, \beta, \Gamma, \Upsilon, r_b, \mu_b, L, f) &= \int dx_{\parallel} d^3 \mathbf{v} v_{\parallel}^2 f(x, v) \\ &= \frac{1}{2} \int_{r^2=\omega^2}^{\infty} \frac{d(r^2)}{\sqrt{r^2 - \omega^2}} \int_{v=0}^{\sqrt{2\psi}} \int_{\eta=0}^{\pi} \int_{\psi'=0}^{2\pi} \\ &\quad \times v^2 dv \sin \eta d\eta d\psi' v^2 \\ &\quad \cdot \left( \cos \eta \frac{\sqrt{r^2 - \omega^2}}{\sqrt{r^2}} + \sin \eta \cos \psi' \sqrt{\frac{\omega^2}{r^2}} \right)^2 f(\epsilon). \end{aligned} \quad (36)$$

This finally takes the form

$$\begin{aligned} N_2(\alpha, \beta, \Gamma, \Upsilon, r_b, \mu_b, L, f) &= 2^{\frac{5}{2}} \left[ 2\pi J_1 \int_0^{1/\omega} \frac{\sqrt{1 - \omega^2 u^2}}{u^2} \right. \\ &\quad \cdot \int_0^{\psi} d\epsilon (\psi - \epsilon)^{\frac{3}{2}} f(\epsilon) + J_2 J_3 \int_0^{\frac{1}{\omega}} \frac{\omega^2}{\sqrt{1 - \omega^2 u^2}} \\ &\quad \left. \cdot \int_0^{\psi} d\epsilon (\psi - \epsilon)^{\frac{3}{2}} f(\epsilon) \right]. \end{aligned} \quad (37)$$

Using the same procedure as was done in the case of power-law galaxies, we compute the LoS velocity dispersion for these galaxies as shown in Fig. 4(d). The distribution function (see Fig. 4(c)) increases towards the higher side of the energy value implying the presence of more high energy stars. Here also the velocity dispersion plot flattens out as we move outwards from the center of the galaxy where the motion of the stars are dominated by the stellar potential.

To simplify our calculation we use the following scales:

$$\rho_s = -\frac{\Upsilon_v}{\pi} \frac{I_b}{r_b}, \quad \psi_s = 4\pi G r_b^2 \rho_s, \quad f_s = \frac{\rho_s}{\sqrt{8\pi^2 m_* \psi_s^{\frac{3}{2}}}}, \quad (38)$$

so that  $\sigma$  is in units of  $\sqrt{\psi_s}$ . In Table 2, we tabulate the values of  $\sigma(\sqrt{Q})$  at radius  $r_e/8$ , where  $r_e$  is the effective radius (Ferrarese & Merritt 2000) and  $Q(\alpha, \beta, \Gamma, r_b, \mu_b) = N_2/D_2$ . The value of  $r_e$  is obtained from

$$\int_0^{r_e} I(R) 2\pi R dR = \frac{1}{2} L_T. \quad (39)$$

#### 4. $M_{\bullet} - \sigma$ relation

By using the data given in Wang and Merritt (2004) for elliptical galaxies as shown in Table 2, we calculate the bulge mass of those galaxies by multiplying the total luminosity by the mass-to-light ratio as prescribed in Magorrian *et al.* (1998). Using equation (16), we calculate the LoS velocity dispersion to get the  $M_{\bullet} - \sigma$  relation by fitting a straight line for 12 galaxies as shown in Fig. 5(a) for different  $f$  values. The  $p$  and  $\log k$  values for different values of  $f$  are shown in the scatter plot (see Fig. 5(b)). From  $\chi^2$  minimization we have determined  $p$  and  $f$ ; the procedure used is shown in a flowchart given in Fig. 6. The formula we used for determining  $\chi^2$  is (Sivia & Skilling 2006)

$$\chi^2 = \sum_k \left[ \frac{(D_k - F_k)^2}{F_k} \right], \quad (40)$$

where a uniform prior is used. The observed values  $D_k$  are obtained for  $M_{\bullet}$  and  $\sigma$  from our calculation using the observational data and the expected value  $F_k$  is obtained by the best-fit straight line to these points as shown in Fig. 5(a). The range of  $f$  and  $p$  has been taken from previous determinations as well as observational values ( $f = 0.001-0.002$ ,  $p = 3-5$ ). The quantity  $S(f, p) \equiv \left( 1 - \frac{\chi^2 - \chi_{\text{min}}^2}{\chi_{\text{max}}^2 - \chi_{\text{min}}^2} \right)$  is in the range 0–1. The

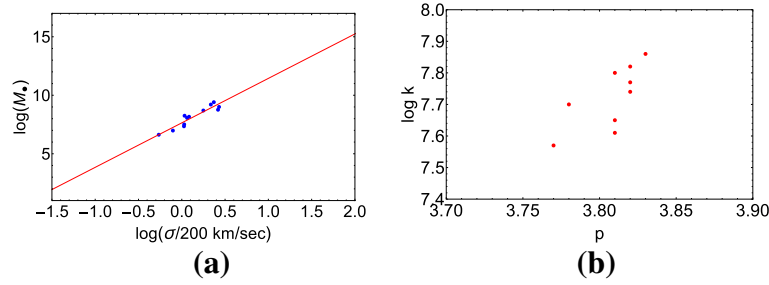


**Figure 5.** The plot of  $\log \sigma$  vs.  $\log M_b$  for 12 galaxies for  $f = 0.0012$ .  $\sigma$  is in units of 200 km/s (a) and (b) the scatter plot of  $p$  and  $\log k$  for different values of  $f$  shows a tight range of  $k$  and  $p$ .

**Table 2.** The first nine columns of the data are used for our calculations ( $r_b$  is the break radius,  $\mu_b$  is the surface brightness, inner slope is  $\Gamma$  and the outer slope is  $\beta$ , sharpness of break is given by  $\alpha$ ,  $\Upsilon$  is the mass-to-light ratio,  $L$  is the total luminosity, the bulge mass  $M_b = \Upsilon_v L$ ) and in the last two columns, the output values of  $r_e$  and the LoS velocity dispersion are shown (Wang & Merritt 2004).

Galaxy	$\log(\frac{r_b}{pc})$	$\mu_b$	$\alpha$	$\beta$	$\Gamma$	$\Upsilon_v(\frac{M_\odot}{L_\odot})$	$\log(\frac{L_v}{L_\odot})$	$\frac{M_b}{10^{10}M_\odot}$	$\log(\frac{r_e}{pc})$	$\sigma$ (km/s)
NGC 3379	1.92	16.10	1.59	1.43	0.18	6.87	10.15	0.90	3.17	230
NGC 3377	0.64	12.85	1.92	1.33	0.29	2.88	9.81	1.86	3.15	217
NGC 4486	2.75	17.86	2.82	1.39	0.25	17.70	10.88	134.30	3.76	433
NGC 4551	2.46	18.83	2.94	1.23	0.80	7.25	9.57	2.69	3.03	218
NGC 4472	2.25	16.66	2.08	1.17	0.04	9.20	10.96	83.90	3.75	542
NGC 3115	2.07	16.17	1.47	1.43	0.78	7.14	10.23	12.12	3.15	230
NGC 4467	2.38	19.98	7.52	2.13	0.98	6.27	8.75	0.35	2.81	108
NGC 4365	2.25	16.77	2.06	1.27	0.15	8.40	10.76	48.34	3.68	524
NGC 4636	2.38	17.72	1.64	1.33	0.13	10.40	10.60	41.40	3.77	354
NGC 4889	2.88	18.01	2.61	1.35	0.05	11.20	11.28	213.4	4.10	469
NGC 4464	1.95	17.35	1.64	1.68	0.88	4.82	9.22	0.80	2.70	157
NGC 4697	2.12	16.93	24.9	1.04	0.74	6.78	10.34	14.83	3.36	215

maximum value of  $S(f, p)$  corresponds to the minimum  $\chi^2$  value. In the plot, we have shown  $S(f, p)$  contours where  $S(f, p) \geq 0.97$  is considered as the allowed range (the red region) for the two parameters and from the plot, we determine the value of  $p = 3.81 \pm 0.004$  and  $f = (1.23 \pm 0.09) \times 10^{-3}$ .

### 5. Summary of results and discussion

We summarize and discuss our key results below.

(1) By assuming the  $M_b - \sigma$  relation as  $M_b = f M_\bullet$  and a single power-law profile for the stellar mass density, we have analytically shown that  $p(\gamma) = (2\gamma + 6)/(2 + \gamma)$  (equation (4)). For a typical a range of  $\gamma = 0.75 - 1.4$ , we find  $p = 3.6 - 5.3$ , which is within the observed range.

(2) The second analysis shown is for the Nuker profile which is a double power law with two slopes  $\beta$  and  $\Gamma$ .

As an approximate analysis, we take an average value of the mean slope to be  $(\beta + \Gamma)/2$  for the set of 12 galaxies (tabulated in Table 2) resulting in  $p = 3.86$  from equation (5), where the value of  $p$  obtained from  $\chi^2$  analysis is 3.81, which is very close. Therefore, our analysis of observational data agrees well with the theoretical expected value.

(3) We have described a procedure for determining the  $M_\bullet - \sigma$  relation (see Fig. 6). Previous models (as discussed in the section 2) determined the  $M_\bullet - \sigma$  relation and also the  $M_b - M_\bullet$  relation independently. We have determined those two relations self-consistently in our model from our  $\chi^2$  analysis (see equation (40)).

(4) For power-law galaxies, we started directly from mass density profile, which in the case of Nuker profile was obtained by inverting the intensity profiles. The  $\sigma$  for different power-law indices are shown in Fig. 2. The variation of  $p$  and  $\log k$  with different values of  $\gamma$ ,  $r_s$  and  $M_s$  are shown in Fig. 3a and Fig. 3b. The variation

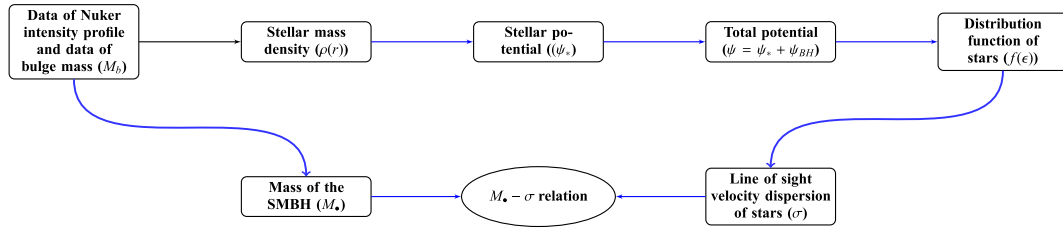


**Figure 6.** The flowchart shows the procedure for calculating the  $M_{\bullet} - \sigma$  relation from the observational data. For the Nuker profile, the stellar mass density is found using Abel inversion and from spherical shell structure the stellar potential is calculated. The SMBH potential is added to get the total potential and the Eddington's formula is used to derive distribution function  $f(\epsilon)$ . The SMBH mass is calculated from the proportionality relation of  $M_b$  and  $M_{\bullet}$ . The path marked by the blue lines only is followed for deriving the  $M_{\bullet} - \sigma$  relation in case of single power-law galaxies.

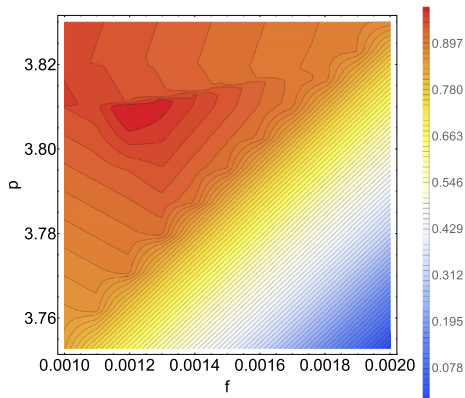


**Figure 7.** The  $S(f, p)$  plot for determination of  $p$  and  $f$  is shown where, the maxima (minima of  $\chi^2$ ) occurs at  $p = 3.81 \pm 0.004$  and  $f = (1.23 \pm 0.09) \times 10^{-3}$ .

of  $\sigma$  with different  $M_{\bullet}$  and  $M_s$  is shown in Fig. 3c and Fig. 3d. For a fixed value of  $\gamma$ ,  $\log k$  and  $\sigma$  depend on the value of  $M_s$  and  $r_s$ . These various diagnostics enable us to interpret the relation by using observables such as  $\gamma$  and  $M_s$  and to predict  $k$  and  $p$ . From observational Nuker intensity profiles, we have determined the LoS velocity dispersion of the stars in the galaxy through their distribution function (see Fig. 4(c), 4(d)). By using a proportionality relation between  $M_b$  and  $M_{\bullet}$ , we have derived values of  $p$  and  $\log k$  for different values of  $f$  by a linear fit (see Fig. 5(b) for scatter plot and Fig. 5(a) for the linear fit for a fixed  $f$ ) and through  $\chi^2$  minimization (see Fig. 7) for the Nuker case. From the scatter plot (see Fig. 5b), it is seen even for a small set of galaxies that the  $p$  and  $\log k$  values within a specific range of  $f$  are very close to the observed range; these are consistent with observations. The obtained values are  $p = 3.81 \pm 0.004$  and  $f = (1.23 \pm 0.09) \times 10^{-3}$ .

## 6. Conclusions

We have discussed a procedure of deriving the  $M_{\bullet} - \sigma$  relation along with a proportionality relation of  $M_b$  and

$M_{\bullet}$  starting from observational data by deriving the distribution function  $f(\epsilon)$ . Using our novel approach, we can also determine the index of the nonlinear relation between  $M_b$  and  $M_{\bullet}$  (as mentioned earlier) as well as  $p$  self-consistently. The  $M_{\bullet} - \sigma$  relation is complicated to explain by existing models. The self consistent determination of  $f$ ,  $k$  and  $p$  is the key for improving the models. The resolution of the problem can come from a DF  $f(\epsilon, L_z)$  built for a central BH and constraining a self-consistent dynamical model from which an explanation of  $f M_b = k \sigma^p$  can finally emerge. That needs much more sophisticated analytical and numerical methods applied to both the bulge mass scaling as well as the  $M_{\bullet} - \sigma$  determination.

## References

- Batiste M., Bentz M. C., Raimundo S. I., Vestergaard M., Onken C. A. 2017, ApJL, 838, L10
- Binney J., Merrifield M. 1998, Galactic Astronomy (Princeton, NJ: Princeton Univ. Press)
- Binney J., Tremaine S. 2008, Galactic Dynamics, 2nd ed., Princeton, NJ: Princeton Univ. Press
- Byun Y.-I. *et al.* 1996, AJ, 111, 1889
- Debatista V. P., Kazantzidis S., van den Bosch F. C. 2013, ApJ, 765, 23
- Faber S. M. *et al.* 1997, AJ, 114, 1771
- Ferrarese L. 2002, ApJ, 578, 90
- Ferrarese L., Ford H. 2005, Space Sci. Rev., 116, 523
- Ferrarese L., Merritt D. 2000, ApJ, 539, L9
- Gebhardt K. *et al.* 2000, ApJ, 539, L13
- Graham A. W. 2016, Galactic Bulges, 418, 263
- Graham A. W., Scott N. 2013, ApJ, 764, 151
- Gültekin K. *et al.* 2009, ApJ, 698, 198
- Häring N., Rix H.-W. 2004, ApJ, 604, L89
- King A. 2003, ApJ, 596, L27
- Kormendy J., Ho L. C. 2013, ARA&A, 51, 511
- Magorrian J. *et al.* 1998, AJ, 115, 2285
- Marconi A., Hunt L. K. 2003, ApJ, 589, L21
- McConnell N. J., Ma C.-P. 2013, ApJ, 764, 184



Merritt D., Ferrarese L. 2001, *ApJ*, 547, 140

Silk J., Rees M. J. 1998, *A&A*, 331, L1

Sivia D. S., Skilling J. 2006, *Data analysis: A Bayesian tutorial*, Oxford: Oxford University Press, p. 64

Stone N. C., Metzger B. D. 2016, *MNRAS*, 455, 859

Tremaine S. *et al.* 2002, *ApJ*, 574, 740

Wang J., Merritt D. 2004, *ApJ*, 600, 149

Zhao H., Haehnelt M. G., Rees M. J. 2002, *New A*, 7, 385